Antiferromagnetic Ordering in $GdRhIn_5$

Kazimierz Łątka[a], Roman Kmieć[b], Michał Rams[a], Andrzej W. Pacyna[b], Vasyl' I. Zaremba[c,d], and Rainer Pöttgen[d]

[a] Marian Smoluchowski Institute of Physics, Jagiellonian University, Reymonta 4, 30-059 Kraków/Poland
[b] Henryk Niewodniczański Institute of Nuclear Physics, Polish Academy of Sciences, Radzikowskiego 152, 31-342 Kraków/Poland
[c] Inorganic Chemistry Department, Ivan Franko National University of Lviv, Kyryla and Mephodiya Street 6, 79005 Lviv/Ukraine
[d] Institut für Anorganische und Analytische Chemie, Westfälische Wilhelms-Universität Münster, Corrensstraße 8, D-48149 Münster/Germany

Reprint requests to R. Pöttgen. E-mail: pottgen@uni-muenster.de

Z. Naturforsch. **59b,** 947 – 957 (2004); received May 17, 2004

Dedicated to Professor Kurt O. Klepp on the occasion of his 60th birthday

A polycrystalline sample of tetragonal $GdRhIn_5$ ($HoCoGa_5$ type, space group $P4/mmm$) was obtained by induction melting of the elements in a glassy carbon crucible in a water-cooled sample chamber and subsequent annealing at 670 K. X-ray powder data yielded the cell parameters $a = 460.65(7)$, $c = 743.52(12)$ pm. The magnetic and electronic properties of $GdRhIn_5$ have been studied by magnetic susceptibility, electrical resistivity, and ^{155}Gd Mössbauer spectroscopic measurements. Antiferromagnetic ordering is detected at 41.0(2) K. The results are discussed using a simple molecular field approximation.

Key words: Indide, Solid State Synthesis, Mössbauer Spectroscopy

Introduction

The series of $RETIn_5$ intermetallics (*RE* = rare earth element, *T* = Co, Rh, Ir) with $HoCoGa_5$ type structure [1, 2] has intensively been investigated in the last five years with respect to their outstanding physical properties. Especially the cerium-based compounds have attracted considerable interest due to the discovery of superconductivity and heavy fermion behavior [3 – 7]. Prominent examples are the 2.3 K heavy fermion superconductor $CeCoIn_5$ [5] and the 3.8 K heavy fermion antiferromagnet $CeRhIn_5$ [7]. The crystal chemistry and the physical properties of this interesting class of compounds have been summarized in a review article [8].

Most of the $RETIn_5$ indides contain stable trivalent rare earth metals [9, 10], however, our recent studies on the ytterbium compounds $YbTIn_5$ (*T* = Co, Rh, Ir) [11, 12] revealed mixed-valent or divalent ytterbium. A useful technique to investigate the valence of the rare earth metal and the magnetic hyperfine interactions is Mössbauer spectroscopy. Mössbauer investigations of Gd-based compounds are particularly relevant since the $4f$ shell of the Gd^{3+} ion is half filled with seven electrons in a spherically symmetric arrangement with zero orbital magnetic moment. Therefore the crystal-field anisotropy does not play a dominant role. In this case, the $4f$ contribution to the electric field gradient (EFG) at the Gd nuclear site can be neglected so then the EFG is entirely due to its lattice part which is determined by the arrangement of ionic and electronic charges around this site. In turn, the lattice part of the EFG is directly related to the B_2^0 term of the crystalline electric field (CEF) Hamiltonian for the $4f$ electrons of rare earth ions with nonzero orbital momentum. The B_2^0 term has usually the major influence on the magnetocrystalline anisotropy for compounds with a tetragonal structure. Hence, its estimation that can be derived from the value of the quadrupole interaction at the Gd nuclei, as observed by Mössbauer spectroscopy, is of great interest. Furthermore, ^{155}Gd Mössbauer effect measurements allow the determination of a polar θ-angle between the direction of the magnetic hyperfine field H_{hf} and the *z*–axis of the EFG. Because of the lattice origin of the EFG for Gd compounds, the *z*-axis of the EFG for crystals with tetragonal point

symmetry of the Gd site points in the direction of the fourfold c-axis. In such a way, the θ-angle determines the easy direction of magnetization. It is worth noting, that Mössbauer spectroscopy is a very helpful tool for microscopic investigations of magnetism and magnetic structures observed within Gd compounds and phases since neutron scattering methods fail owing to the prohibitively high nuclear cross section of natural Gd.

Herein we report on magnetic and ^{155}Gd Mössbauer studies of the 44 K antiferromagnet $GdRhIn_5$ [9]. This indide was first reported at a conference [13].

Experimental Section

Synthesis

Starting materials for the preparation of $GdRhIn_5$ were ingots of gadolinium (Johnson Matthey), rhodium powder (200 mesh, Degussa–Hüls) and indium tear drops (Johnson Matthey), all with stated purities better than 99.9%. The elements were weighed in the 1:1:5 atomic ratio and put in a glassy carbon crucible (SIGRADUR®G, glassy carbon, type GAZ006). Rhodium was used in the form of a small cold-pressed pellet (∅ 6 mm). The glassy carbon crucible was put in a protective quartz tube and placed in a water-cooled sample chamber of a high-frequency furnace [14]. The elements were then reacted by induction melting under flowing argon. The argon was purified before over molecular sieves, silica gel and titanium sponge (900 K). The indium melted first and formed an alloy with rhodium, and then this alloy reacted at higher temperature with gadolinium. After the reaction the sample was kept at around 1300 K for 15 min and was subsequently cooled to 800 K within 30 min. Finally the sample was quenched by turning off the high-frequency power. The sample could easily be separated from the crucible. No reactions with the glassy carbon could be detected. The sample was then sealed in an evacuated silica tube and annealed at 670 K for four weeks.

The purity of the melted and annealed $GdRhIn_5$ samples was checked through Guinier powder patterns using Cu-$K_{\alpha 1}$ radiation and α-quartz ($a = 491.30$ pm, $c = 540.46$ pm) as an internal standard. To ensure correct indexing, the experimental powder pattern was compared with a calculated one [15] using the atomic parameters of $YbRhIn_5$ [12]. The lattice parameters were obtained from least-squares fits of the Guinier data: $a = 460.65(7)$, $c = 743.52(12)$ pm. These parameters are in good agreement with our previous data [13] ($a = 460.1$, $c = 744.5$ pm) as well as the data given by Pagliuso *et al.* ($a = 460.9(4)$, $c = 744.4(7)$ pm) [10].

Magnetic and transport measurements

Magnetic susceptibility and magnetization measurements were carried out with a SQUID magnetometer (Quantum Design MPMS) and a 7225 Lake Shore susceptometer operating in AC mode on powdered samples. SQUID measurements were performed in the temperature range 1.8 – 300 K and in fields up to 5 T. AC studies were done between 4.5 and 100 K. The complex AC susceptibility technique is a precise tool for reliable determination of phase transition temperatures since magnetic measurements can be made under zero external field regimes and at sufficiently low strengths of AC fields not significantly affecting the magnetic order parameter. In addition also the second χ_2, third χ_3, and fifth χ_5 harmonics were measured in order to get deeper insight into the character of the phase transition. The temperature dependence of all magnetic effects was measured first in zero field cooling (ZFC) mode while in the field cooled (FC) mode an external magnetic field was switched on above the transition temperature.

Electrical resistivity

Only qualitative resistivity measurements were made on a bulk probe using a steady-current, standard four point technique. Small wires were glued with silver paste to a bar-shaped specimen of about $3 \times 3 \times 2$ mm^3.

^{155}Gd Mössbauer spectroscopy

^{155}Gd Mössbauer spectra were collected in a transmission geometry cryostat using a conventional constant-acceleration spectrometer of the Kankeleit type. The 20 mCi ^{155}Eu:$SmPd_3$ source (86.5 keV ($I_g = 3/2$, *E1*, $I_e = 5/2$ transition) was kept at 4.2 K to increase the efficiency of the resonance emission. The temperature of the absorber was varied between 4.2 and 47 K with a stability better than 0.05 K. The absorber was made of the powdered material placed in a thin-walled (0.1 mm) aluminium disk container to ensure a significant transmission for γ rays and a homogeneous temperature over the whole sample. The used absorber thickness of about 344 mg/cm^2 was close to the value of 332 mg/cm^2 obtained from the optimization procedure [16, 17] under the assumption that the absorber Debye-Waller factor f_a is 5% *i.e.* a value typical for Gd intermetallics. The resonance 86.5 keV γ rays were detected by a scintillation NaI(Tl) counter (3 cm thick). A 0.9 mm thick Pb foil was applied as critical absorber to reduce the higher 105.3 keV γ-ray transition. The drive velocity calibration was performed with a ^{57}Co(Rh) source against a standard metallic iron foil at room temperature.

The analysis of the experimental resonance line shapes was carried out using the transmission integral formula with a numerical diagonalization routine of the full hyperfine Hamiltonian [18]. The asymmetry parameter $\eta = (V_{xx} - V_{yy})/V_{zz}$ was put to zero owing to the tetragonal symmetry of the Gd site. In this case the spectral shape does not depend on the polar angle φ. The source width Γ_s of the recoil-free emit-

ted γ line and the background reduced Debye-Waller factor of the source, f_s, were determined from an independent measurement with a standard $GdFe_2$ absorber. They were kept constant during all fits to the experimental spectra while the nuclear g-factor ratio, g_{ex}/g_g, and the ratio of nuclear quadrupole moments, Q_{ex}/Q_g, were constrained to 1.235 and 0.087 [19], respectively. The interference ξ-factor for the E1 transition of 86.5 keV was fixed to the value $\xi = 0.0275$ [18] in the absorption cross-section.

Results and Discussion

Crystal chemistry

$GdRhIn_5$ crystallizes in the relatively simple $HoCoGa_5$ type structure [1], space group $P4/mmm$. The unit cell and the coordination polyhedra (drawn with the In2 z parameter of $YbRhIn_5$ [11]) are shown in Fig. 1. The gadolinium and In1 atoms have coordination number 12 in a cuboctahedral arrangement with site symmetry $4/mmm$; Gd with 12 indium atoms and In1 with 8 In and 4 Gd neighbors. The rhodium atoms have eight indium neighbors in a slightly distorted cubic coordination ($4/mmm$). The In2 atoms have the lowest site symmetry, $2mm$, with seven indium, two rhodium, and two gadolinium atoms in their coordination shell. The structure is characterized by strong Rh–In and In–In bonding. From a geometrical point of view, the structure can be described by a stacking of two different layers, *i.e.* condensed $GdIn_{12}$ cuboctahedra around $z = 0$ and condensed $RhIn_8$ cubes around $z = 1/2$. For further details on the crystal chemistry of the $RETIn_5$ intermetallics we refer to previous work [1, 2, 8].

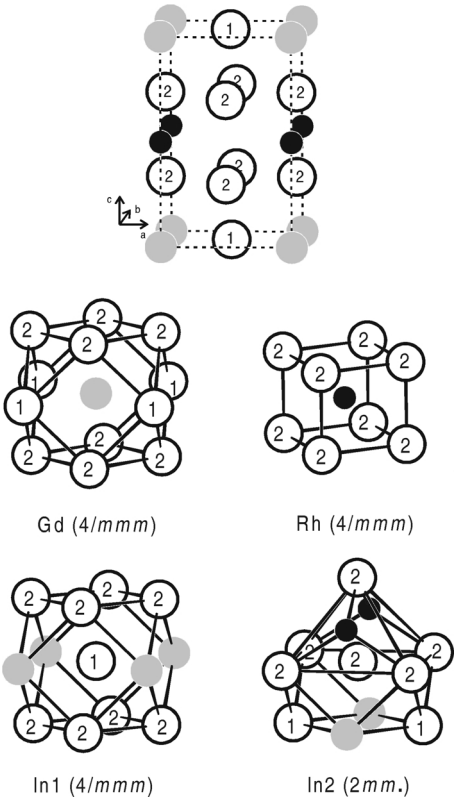

Fig. 1. Unit cell (top) and coordination polyhedra (bottom) of the $GdRhIn_5$ structure. The gadolinium, rhodium, and indium atoms are drawn as grey, filled, and open circles, respectively. Atom designations and site symmetries are indicated.

Bulk magnetic properties – SQUID results

The results of magnetic susceptibility and magnetization studies are displayed in Figs. 2–8. The temperature dependence of the static magnetic susceptibility (Fig. 2) was measured in an external field of 1 kOe and in the temperature range 1.8 – 300 K. The most prominent feature in $\chi(T)$ (left-hand scale in Fig. 2) is the pronounced maximum associated with a distinct minimum in the inverse magnetic susceptibility $\chi^{-1}(T)$ (right-hand scale in Fig. 2) at $T = 40.0(5)$ K indicating the transition to the antiferromagnetic state. The transition temperature is in a perfect agreement with the Néel temperature $T_N = 40$ K found by Pagliuso *et al.* [10]. In the paramagnetic region, the susceptibility follows a Curie-Weiss law $\chi(T) = C/(T - \theta_p)$ with the effective magnetic moment $\mu_{eff} = 2.83(C_M)^{1/2} = 8.40\ \mu_B$ (where $C_M = 8.82$ cm^{3}K/mol is the molar Curie constant; $C_M = MC$ and M is the molar mass), and

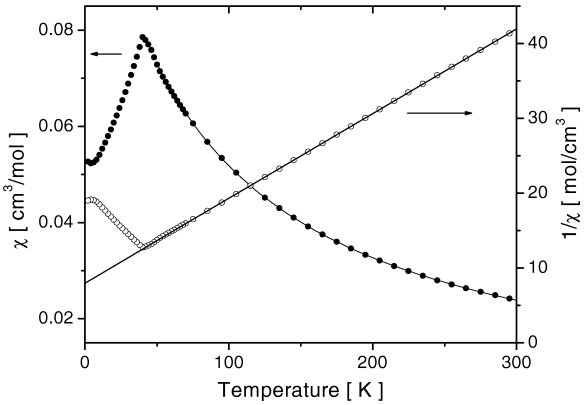

Fig. 2. Temperature dependence of the susceptibility (left-hand scale) and the reciprocal susceptibility (right-hand scale) of $GdRhIn_5$ measured at an external field of 1 kOe.

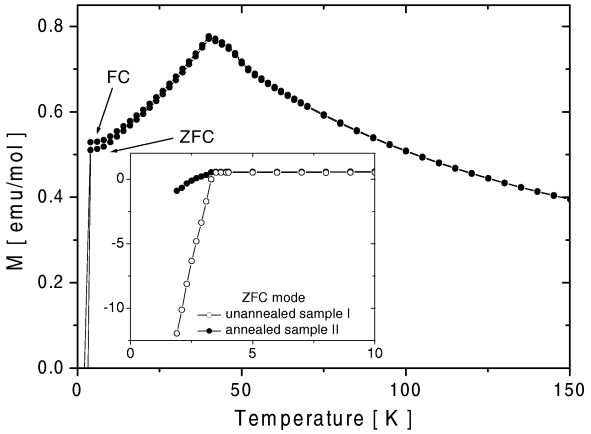

Fig. 3. Zero-field cooled (ZFC) and field-cooled (FC) magnetizations measured in a static field $H_0 = 10$ Oe as a function of temperature for the annealed $GdRhIn_5$ sample. The low temperature ZFC magnetic behaviour is reproduced for comparison in a larger scale in the insert for the unannealed sample I (open circles) and the annealed sample II (filled circles). For details see text.

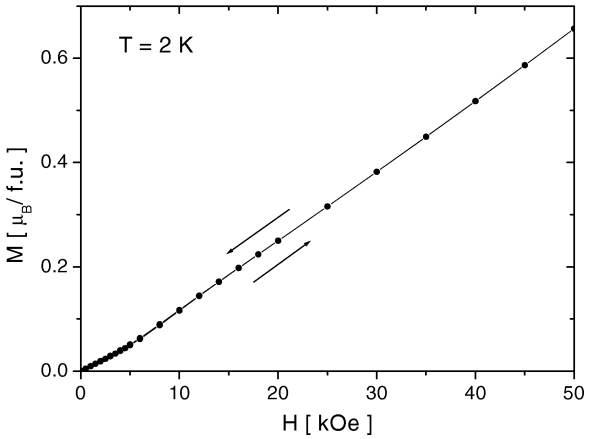

Fig. 4. Field dependence of the magnetization M per formula unit measured with increasing and decreasing external magnetic field for $GdRhIn_5$ at $T = 2.0$ K, started after zero-field cooling (ZFC) of the sample.

the paramagnetic Curie temperature $\theta_p = -70(1)$ K. The observed effective magnetic moment is remarkably higher than the theoretical value characteristic for a free Gd^{3+} ion described by $\mu_{eff}{}^{theor} = \mu^{(4f)} = g\,\mu_B[(J+1)]^{1/2} = 7.94\ \mu_B$. The resulting excess moment, induced *via* $4f$-5*d* exchange interactions, is usually ascribed to a contribution from *d*-electrons originating mainly from the gadolinium ions (see discussion and references in [20–23]). Since this excess magnetic moment is correlated with the $4f$ Gd magnetic moment $\mu^{(4f)}$, and μ_{eff} is given by the sum of the $\mu^{(4f)}$ and $\mu^{(5d)}$ magnetic contributions, therefore, the upper bound for $\mu^{(5d)}$ of the Gd-5*d* magnetic contribution is estimated by subtraction of the theoretical value $\mu^{(4f)}$ from the $\mu_{eff}{}^{exp}$ what gives $\mu^{(5d)} = 0.46\ \mu_B$.

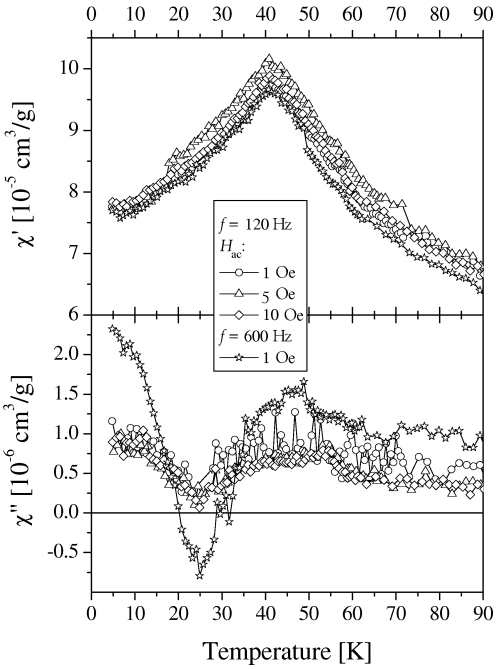

Fig. 5. Zero-field susceptibilities $\chi'(\omega)$ and $\chi''(\omega)$ of $GdRhIn_5$ recorded simultaneously as a function of temperature with internal frequencies of 120 and 600 Hz, respectively, and oscillating field amplitudes H_{AC} ranging from 1 to 10 Oe.

The strongly negative value of θ_p acquired for $GdRhIn_5$ undoubtedly manifests antiferromagnetic interactions in this compound. The striking feature of the magnetic susceptibility shown in Fig. 2 is that the ratio of the powder susceptibility at absolute zero to that at the Néel point $\chi(0)/\chi(T_N) = 0.0528/0.0785$ (where $\chi(0)$ was obtained from extrapolation of the experimental value of χ to 0 K) is approximately 0.67 and agrees perfectly well with the value predicted for a polycrystalline sample [24], where $\chi(0) = (2/3)\ \chi_\perp$ and $\chi(T_N) = \chi_\perp$ giving the ratio $\chi(0)/\chi(T_N) = 2/3 \approx 0.67$. This was a first hint that antiferromagnetic ordering in $GdRhIn_5$ has a simple character as confirmed by further experiments (see below).

Results of zero-field cooled (ZFC) and field-cooled (FC) magnetizations measured in the static field $H_0 = 10$ Oe as a function of temperature for the annealed $GdRhIn_5$ sample are shown in Fig. 3. The low temper-

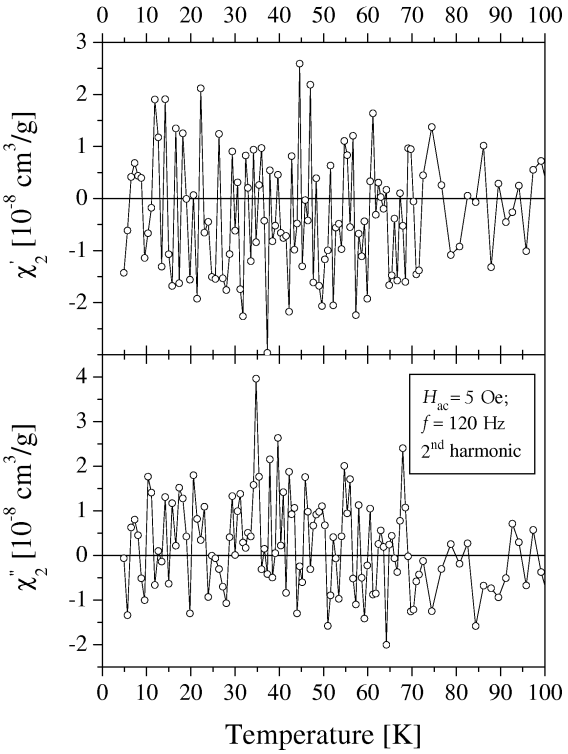

Fig. 6. Temperature dependence of the signal intensities of the 2nd harmonics χ_2' and χ_2'', respectively, registered with an internal frequency of 120 Hz for $GdRhIn_5$. Data were collected after the ZFC process with an oscillating field H_{AC} = 5 Oe.

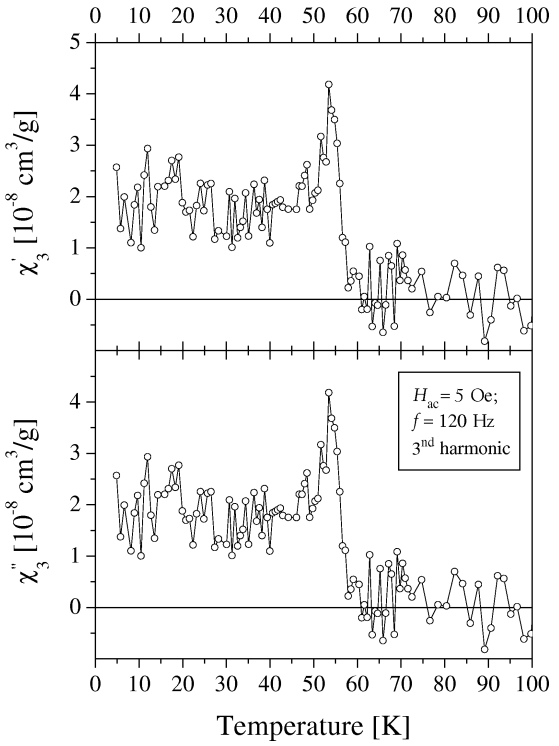

Fig. 7. Temperature dependence of the signal intensities of the 3rd harmonics χ_3' and χ_3'', respectively, registered with an internal frequency of 120 Hz for $GdRhIn_5$. Data were collected after the ZFC process with an oscillating field H_{AC} = 5 Oe.

ature ZFC magnetic behavior is reproduced for comparison in a larger scale in the insert for the unannealed sample I (open circles) and the annealed sample II (filled circles). The unannealed sample is the one obtained after the heat treatment in the induction furnace. The rapid fall of the magnetization observed at $T_c = 3.4$ K can be associated with a superconducting transition of a tiny admixture of pure metallic indium, probably at the grain boundaries of the polycrystalline sample. The amount of the indium impurity was estimated from FC measurements on the investigated annealed sample to be of about 0.6% where the entire change of magnetization at the transition temperature T_c was prescribed only to metallic In. It is clearly seen from the insert in Fig. 3 that the annealing process strongly diminishes the In impurity. All further property evaluations refer to the annealed sample.

Fig. 4 presents the field dependence of the magnetization M per formula unit measured with increasing and decreasing external magnetic field at $T = 2.0$ K starting after zero-field cooling of the sample. An upturn observed in the magnetization curve $M(H)$ in the low field region can be interpreted as a spin-flop transition at H_{SF} of *ca.* 5 kOe. Since our measurements were performed with polycrystalline material, the spin-flop transition does not occur abruptly at a sharply defined field H_{SF} but is spread over a range of fields, and H_{SF} can be estimated as an average value. A linear behavior of the magnetization above H_{SF} is a characteristic feature for a simple antiferromagnet.

Bulk magnetic properties – AC magnetic susceptibility

The results of the AC magnetic susceptibility measurements are displayed in Figs. 5 – 8. The real $\chi'(T)$ and imaginary $\chi''(T)$ parts of the magnetic susceptibility were measured simultaneously as a function of temperature at zero external magnetic field with internal frequencies of 120 and 600 Hz, respectively, and oscillating field amplitudes H_{AC} ranging from 1 to 10 Oe. (Fig. 5).

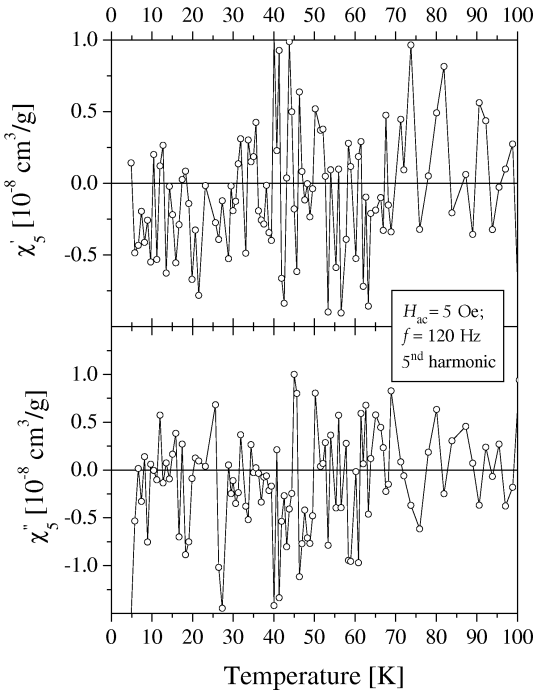

Fig. 8. Temperature dependence of the signal intensities of the 5th harmonics χ_5' and χ_5'', respectively, registered with an internal frequency of 120 Hz for $GdRhIn_5$. Data were collected after the ZFC process with an oscillating field H_{AC} = 5 Oe.

The registered $\chi'(T)$ maxima at $T = 41.0(2)$ K correspond to the antiferromagnetic phase transition found at $T = 40.0(5)$ K by SQUID measurements (Fig. 2) although, they are a little shifted towards higher temperature. Because AC measurements were made with better precision owing to a more precise temperature scanning, this temperature is ascribed here as the Néel temperature T_N. An absence of a peak in $\chi''(T)$ clearly points to collinear antiferromagnetic ordering in $GdRhIn_5$. This finding is further corroborated by the lack of any anomaly around 41 K in the second χ_2, third χ_3, and fifth χ_5 harmonics of magnetic susceptibility shown in Figs. 6–8, respectively.

Electrical resistivity

The resistivity measurements for $GdRhIn_5$ are shown in Fig. 9. It is interesting to point out that below and above the Néel temperature $T_N = 41$ K, the resistivity of this material presents, to a good approximation, a power law behaviour, $\rho \propto T$, presented by two straight lines fitted to the experimental points in the low and high temperature region. The intersection

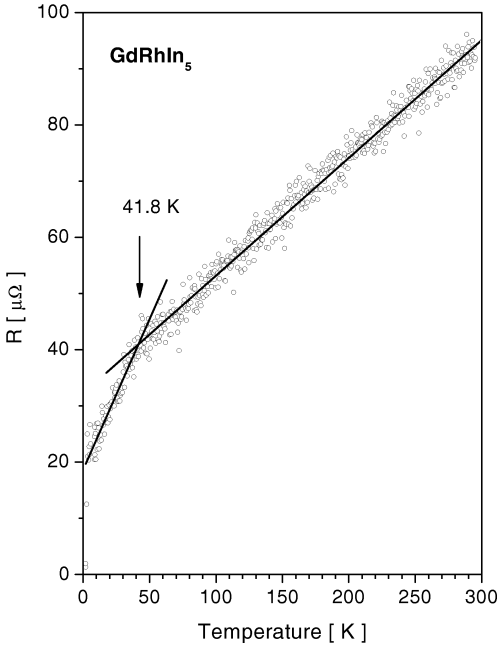

Fig. 9. Temperature dependence of the electrical resistivity ρ(T). The arrow at $T_c^{\rho} = 41.8$ K indicates an intersection of two straight lines fitted to the experimental points below and over the Néel temperature $T_N = 41$ K. For details see text.

of these two lines at $T_c^{\rho} = 41.8$ K that agrees well with the Néel temperature $T_N = 41$ K can be taken as a kind of the resistivity transition temperature. Such a power law in the magnetic state is consistent with an S-state of the Gd ions. In the paramagnetic region the linear increase of the resistivity arises from dominant electron-phonon interactions.

^{155}Gd Mössbauer spectroscopy

The hyperfine parameters obtained from the least-squares fits of the transmission integrals to the experimental data are listed in Tables 1 and 2. Two repre-

Table 1. Hyperfine interaction parameters obtained from the ^{155}Gd resonance spectrum of $GdRhIn_5$ obtained at T = 47 K *i.e.* above the Néel temperature. For explanations see text. For the 86.5 keV γ transition in ^{155}Gd, 1 mm/s corresponds to $28.868(1) \cdot 10^{-8}$ eV or 69.803(3) MHz.

Fit number	δ_{is}[a] [mms^{-1}]	$\lvert\Delta E_Q$[b]$\rvert$ [mms^{-1}]	Γ_A [mms^{-1}]	χ^2
1	0.654(1)	0.182(2)	0.204(3)	1.056
2	**0.657(2)**	**0.171(2)**	**0.25**[c]	**1.271**

[a] δ_{is} is relative to the (^{155}Eu)$SmPd_3$ source; [b] $\Delta E_Q = eQV_{zz}/4$; [c] parameter kept constant during the fit procedure and equal to the natural linewidth $\Gamma_n = 0.25$ mm/s [25]. For explanations see text.

Table 2. Hyperfine interaction parameters obtained by various fit procedures from the analysis of the ^{155}Gd Mössbauer spectrum recorded for $GdRhIn_5$ at 4.2 K. For explanations see text. For the 86.5 keV γ transition in ^{155}Gd, 1 mm/s corresponds to $28.868(1)\cdot 10^{-8}$ eV or 69.803(3) MHz.

Fit number	δ_{is} [a] [mms^{-1}]	$\lvert\Delta E_Q\rvert$ [b] [mms^{-1}]	$\lvert H_{hf}\rvert$ [kOe]	θ [°]	Γ_A [mms^{-1}]	χ^2
1	0.659(3)	+0.171[c]	232.2(9)	42.0(1.6)	0.25[c]	2.240
2	0.660(2)	−0.171[c]	233.5(7)	97.0(3.6)	0.25[c]	1.468
3	**0.660(2)**	**−0.171**[c]	**233.4(7)**	**90.0**[c]	**0.25**[c]	**1.467**
4	0.659(2)	−0.166(10)	233.3(8)	95.9(4.8)	0.25[c]	1.472
5	0.659(2)	−0.163(9)	233.2(8)	90.0[c]	0.25[c]	1.468

[a] δ_{is} is relative to the (^{155}Eu)$SmPd_3$ source; [b] $\Delta E_Q = eQV_{zz}/4$; [c] parameters kept constant during the fit procedure. For explanations see text.

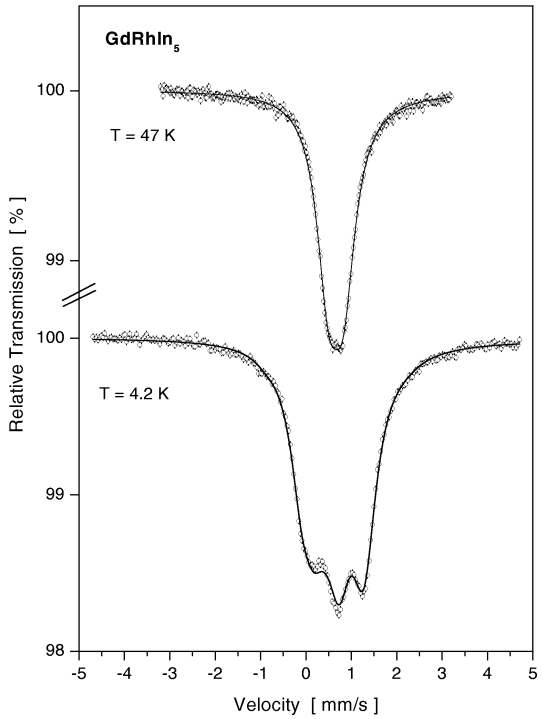

Fig. 10. ^{155}Gd resonance spectra for $GdRhIn_5$ recorded at 47 and 4.2 K. The continuous lines represent the least-squares fits to the experimental points.

sentative experimental spectra are displayed in Fig. 10. The upper spectrum recorded at $T = 47$ K, *i.e.* above T_N, reveals the typical quadrupole splitting and can be fitted with a singular quadrupolar hyperfine pattern characteristic for paramagnetic Gd^{3+} in non-cubic site symmetry, without any impurity contribution. This fully agrees with a single crystallographic gadolinium position as determined by X-ray diffraction. The isomer shift δ_{is} was determined with respect to the ^{155}Eu:$SmPd_3$ source and its value is almost the same for both fits presented in Table 1. In fit number 1, all parameters were refined without constraints. Although the quality fit factor χ^2 is better than that for the second fit, this fit must be rejected since the derived value for the absorption linewidth of $\Gamma_A = 0.204(3)$ mm/s is unphysical. It is significantly reduced when compared to the natural linewidth $\Gamma_n = 0.25$ mm/s [25]. For that reason, in all other fits the absorption linewidth Γ_A was always constrained to the value of the natural linewidth Γ_n.

The sign of the quadrupole interaction constant $\Delta E_Q = eQV_{zz}/4$ (where $Q = (1.30 \pm 0.02)b$ [26] is the quadrupole moment of the nuclear ground state and V_{zz} is the z-component of the electric field gradient (EFG) tensor) cannot be derived from this spectrum. The value of the quadrupole moment in the excited state ($I_e = 5/2$) is small since the consecutive quadrupole splitting of that level is much smaller than the natural linewidth. Therefore, only the absolute value of the quadrupole splitting parameter $|\Delta E_Q|$ can be obtained from the fitting procedure.

The spectrum taken at $T = 4.2$ K (Fig. 10), *i. e.* much below the antiferromagnetic transition, was analysed carefully in order to get a reliable set of hyperfine parameters for a proper description of the temperature evolution of the spectra observed between $T = 4.2$ K and the Néel temperature $T_N = 41$ K. It was found that satisfactory fits can be obtained with a single magnetically split component which points to a single magnetic position of the Gd ions in the magnetic structure. The results obtained by various fit procedures are summarized in Table 2. The absolute value of the quadrupole interaction constant $|\Delta E_Q|$ was limited to that derived in the paramagnetic state at $T = 47$ K (Table 1) in the fits described by numbers $1-3$. This is justified by the poor spectral resolution of ^{155}Gd Mössbauer spectroscopy and a rather strong correlation between this parameter, and the polar angle θ. As a matter of fact, even if ΔE_Q is treated as a free parameter one can get reasonable fits (fits number 4 and 5) with slightly smaller absolute values $|\Delta E_Q|$ (Table 2) which are, however, comparable to the value obtained at $T = 47$ K. As it is evident from Table 2, fit number 1 with a positive sign of ΔE_Q is definitely worse than those with negative ones (fits $2-5$), and therefore the negative sign was chosen to fit the other magnetically split spectra. Simultaneously, the values derived for isomer shifts δ_{is} as well as magnetic hyper-

fine fields are almost the same within the experimental errors. They do not depend on other parameters.

Special attention was paid to the derivation of the polar angle θ, since it manifests the easy axis of magnetization. Closer inspection of Table 2 (fits 2–4) shows that this angle is equal or near 90°. It means that the magnetic Gd moments, which follow the magnetic hyperfine field direction, are confined in or close to the plane perpendicular to the *c*-axis, and this plane can be recognized as the easy plane of magnetization. Hence, our magnetic and spectroscopic results lead to an antiferromagnetic collinear magnetic structure of $GdRhIn_5$ with magnetic Gd moments aligned in or close to the basal plane. It is then tempting to assume that the magnetic structure consists, for example, of ferromagnetic Gd planes perpendicular to the *c*-axis which are stacked in a sequence + – + – providing net antiferromagnetic order.

The isomer shift δ_{is} is caused by a change in the nucleus size during the nuclear transition. It can be expressed in the form $\delta_{is} \sim \Delta\langle r^2\rangle_{nucl}\ (|\psi_A|^2 - |\psi_S|^2)$, where $\Delta\langle r^2\rangle_{nucl}$ is the difference between the mean-square nuclear radii involved in the Mössbauer transition, and $|\psi_A|^2$, $|\psi_S|^2$ denote electron densities at the site of the nucleus for the absorber and the source, respectively. The isomer shift (Table 2) is slightly decreasing with increasing temperature. Since the quantity $\Delta\langle r^2\rangle_{nucl}$ is negative [27] for the 86.5 keV transition in ^{155}Gd, therefore, the observed large positive isomer shift is associated with respectively smaller electron density at the absorber nucleus in comparison to the electron density at the source nucleus. One can then anticipate that an increase of the isomer shift implies a reduction of the electronic density at the ^{155}Gd nuclei in the absorber, and vice versa. Such a reduction can be caused by a reduced population of 6*s* states at the Gd sites, and/or from a 6*s*-to-5*d* transfer. An increase of the atomic volume may also lead to reduced electron density at the absorber nuclei and thus to a more positive isomer shift.

The quadrupole interaction constants $\Delta E_Q = eQV_{zz}/4$ (Tables 1 and 2) can be easily converted into the values of the electric field gradient (EFG) V_{zz} at the gadolinium nuclei by the formula: $V_{zz} = 8.8826 \cdot 10^{21}\ \Delta E_Q$ [mm/s] V/m^2. Hence, the accepted value $\Delta E_Q = -0.171(2)$ mm/s corresponds to $V_{zz} = -1.52(2) \cdot 10^{21}$ V/m^2. Furthermore, knowledge of the EFG at the Gd site allows an estimation of the quadrupolar term B_2^0 in the Stevens expansion of the crystal field *Hamiltonian*: $\sum B_n^m O_n^m$. This term is directly related to $\Delta E_Q(^{155}\mathrm{Gd})$ by the expression:

$$B_2^0\,[\mathrm{K}] = -\alpha_J \cdot \langle r^2\rangle_{4f} \cdot 361 \cdot \Delta E_Q(^{155}\mathrm{Gd})$$

Here, α_J is the appropriate Stevens factor, and the mean squared radius $\langle r^2\rangle_{4f}$ is expressed in atomic units and ΔE_Q in mm/s. If the B_2^0 parameter is dominant then its sign gives a hint to the direction of the rare earth magnetic moment in the isostructural $RERhIn_5$ compounds where the rare earths metals have non-zero angular momentums [28–30]. For a positive value of the B_2^0 parameter the basal plane ($\perp z$) is preferred for the moment direction while for a negative value an ordering along the *z* axis is anticipated. For Ce and Nd the Stevens factors α_J are negative while for Sm α_J is positive leading to negative B_2^0 parameters in the case of $CeRhIn_5$ and $NdRhIn_5$, and a positive B_2^0 value for $SmRhIn_5$. This means that the anticipated orientation of the magnetic moments for the Ce and Nd compounds are along the *c*-axis, and perpendicular for the Sm compound. This has indeed experimentally been confirmed [10] (and ref. therein). This observation strongly suggests that the B_2^0 term is dominant for the tetragonal $RERhIn_5$ compounds.

The temperature variation of the magnetic hyperfine field H_{hf} is shown in Fig. 11. The continuous temperature evolution of $|H_{hf}(T)|$ is described in the frame of a molecular field approximation by a $S = 7/2$ Brillouin function. The Curie temperature $T_N{}^M = 38.4$ K

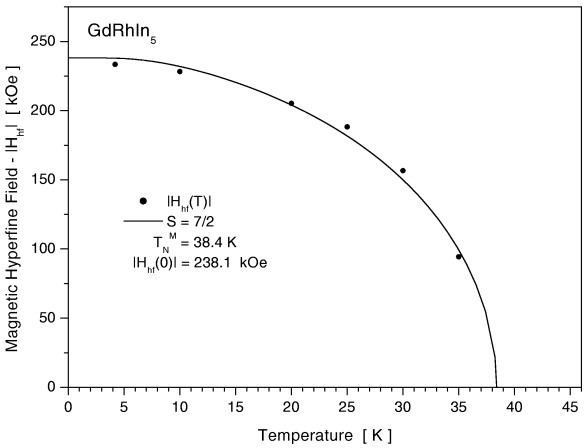

Fig. 11. Temperature evolution of the magnetic hyperfine field $|H_{hf}|$ at the gadolinium site for $GdRhIn_5$. The continuous line represent the least-squares fit of the Brillouin function for $S = 7/2$. The fit gives the estimated Néel temperature $T_N{}^M = 38.4$ K and the absolute value of the saturated magnetic hyperfine field $|H_{hf}(0)| = 238.1$ kOe.

is somewhat lower than that obtained from magnetic measurements, $T_N = 41$ K. The saturation magnetic hyperfine field $|H_{hf}(0)|$ is 238.1 kOe. The magnetic hyperfine field at the gadolinium nucleus $\boldsymbol{H_{hf}}$ can be decomposed into two terms, $\boldsymbol{H_{hf}} = \boldsymbol{H_{CP}} + \boldsymbol{H_{CE}}$. $\boldsymbol{H_{CP}}$ is the field due to core polarization by the local $4f$ moment and $\boldsymbol{H_{CE}}$ is the field due to the conduction electron polarization consisting of the two contributions $\boldsymbol{H_s}$ and $\boldsymbol{H_{tr}}$. $\boldsymbol{H_s}$, known as the self-polarization term, is ascribed to the polarization of conduction electrons by the local Gd magnetic moment and the transferred field, $\boldsymbol{H_{tr}}$, induced by neighbouring Gd magnetic moments, is created by the polarization of the conduction electrons *via* RKKY interactions as well as by the dipolar field. The core polarization value, $H_{CP} = -340(20)$ kOe [31, 32] is assumed to be independent of the Gd environment in solids. The orbital field, the dominant contribution for most other rare earths, is negligible for Gd, and also, the dipolar field, which is generally non-zero for tetragonal symmetry, is neglected to a first approximation. Assuming that the measured magnetic hyperfine field H_{hf} is negative (as observed for Gd intermetallics), one can conclude that the total contribution from the polarization of the conduction electrons $H_{CE} = H_{hf} - H_{CP} = -238.1\text{ kOe} - (-340\text{ kOe}) = 101.9$ kOe is positive.

Magnetic interactions

The strength of the exchange interactions between the magnetic moments is reflected in the paramagnetic Curie-Weiss temperature θ_p and in the ordering temperature T_N. In the framework of molecular field theory, leading to the Curie Weiss law, θ_p is proportional to the sum over the exchange integrals between all pairs of moments. In the case of collinear antiferromagnetic order, T_N can be expressed in a similar way with a change of sign for the terms relating to pairs of moments pointing in opposite directions [33]. For non-collinear ordering, T_N is related to the exchange integrals in a more complex way. The exact derivation of the interaction energies is not possible as the real magnetic structure of $GdRhIn_5$ is not known. Nevertheless, the most relevant interaction energies can be estimated on the basis of a two-sublattice molecular field approximation (MFA) for simple antiferromagnets considering the experimentally derived values of T_N and θ_p.

In the MFA the intra-sublattice energy is given by $E_{AA} = 0.5k_B(T_N + \theta_p)$ whereas the inter-sublattice energy is expressed as $E_{AB} = 0.5k_B(T_N - \theta_p)$, leading to $E_{AA} = -1.25$ meV and $E_{AB} = 4.78$ meV. T_N and θ_p can also be expressed by the two molecular constants λ and β by the relations [24] $T_N = 0.5C(\lambda - \beta)$ and $\theta_p = 0.5C(\lambda + \beta)$, where C is the Curie–Weiss constant. Here, λ plays the role of an inter-sublattice interaction molecular constant, which in the MFA should be positive to favour anti-parallel ordering and much greater in the absolute value than the intra-sublattice molecular constant β. Taking into account all equations we can show that: $E_{AA} = -0.5k_BC\beta$ and $E_{AB} = 0.5k_BC\lambda$ or $E_{AB}/E_{AA} = \lambda/\beta \approx -3.8$. In view of the values for E_{AA} and E_{AB} it is clear that our experimental results for T_N and θ_p lead to the constants λ and β which fulfil MFA requirements (*i.e.* λ is positive and the absolute value is greater than β). In the two-sublattice molecular field model, λ is related to the perpendicular susceptibility $\chi_\perp$ through $\chi_\perp \approx 1/\lambda$ or $\lambda \approx 1/\chi_\perp$ [24, 34]. In the MFA $\chi_\perp$ is a constant that is independent of temperature. We find its value from the experiment as equal to the magnetic susceptibility at the Néel temperature, *i.e.* $\chi_\perp = \chi(T_N) = 0.0785$ cm^3/mol (Fig. 2), leading to $\lambda = 12.73$ mol/cm^3. λ can also be estimated independently from the relation $E_{AB} = 0.5k_BC\lambda$. Taking C from the experiment we obtain $\lambda = 12.6$ mol/cm^3 in surprisingly good agreement with the previous value. These simple calculations show that the two-sublattice model is reliable and the results are consistent with the experiments.

The experimentally estimated spin-flop (SF) field $H_{SF} \approx 5$ kOe can be used to estimate an anisotropy field H_A. At $T = 0$, the model treated above gives: $H_{SF} \approx (2H_EH_A)^{1/2}$ [24, 34], where H_E is a molecular field. In the MFA $H_E \approx \lambda M_i$ [24, 34]. With the sublattice magnetization at $T = 0$ given by $M_i = M_0 = 0.5Ng\mu_BS$ (where N is the total number of magnetic ions in the unit volume and $gxS = 7$ for Gd^{3+}) and $\lambda \approx 1/\chi_\perp$ [24, 34] we obtain $H_A \approx {H_{SF}}^2/2H_E \approx {H_{SF}}^2/2\lambda M_0 \approx {H_{SF}}^2\chi_\perp/2M_0$. Taking the experimental data we get $H_A \approx 0.05$ kOe. The magnitude of this anisotropy is reasonable. The magnetic anisotropy of Gd compounds is usually rather small owing to the fact that it originates from a single-ion anisotropy associated with crystal field effects, and that it is caused by small admixtures of excited J-mutiplets $^6P_{7/2}$, $^6D_{7/2}, \ldots$ to the $^8S_{7/2}$ ground state of the Gd shell [35]. Generally, the anisotropy field H_A due to crystal effects on Gd is expected to be smaller than 0.1 kOe, although, these effects may be higher in metallic than in insulating compounds [35]. Dipole-dipole interactions are

another source of magnetic anisotropy but they lead to anisotropy fields of similar magnitude.

The MFA is also useful for the study of phase boundaries. The AF-P phase boundary, when the magnetic field **H** is perpendicular to the easy axis, and the SF-P phase boundary for **H** along the easy axis, are given by the equations $H_{\mathrm{AFP}} = 2\lambda M_i(0,T)$ and $H_{\mathrm{SFP}} = 2\lambda M_i(0,T)$ [36]. In both cases the critical fields $\mathrm{H_{AFP}}$ and $\mathrm{H_{SFP}}$ are predicted to be equal. Hence, at $T = 0$, H_{SFP} (with **H** along the easy axis), for example, is equal to $2\lambda M_0$, leading to $H_{\mathrm{SFP}} = 498$ kOe. This can be a reason why under our experimental circumstances, limited to an external field $H = 50$ kOe, SF-P transitions can not be realized at low enough temperatures, and a linear magnetization with increasing magnetic field is observed.

Conclusions

In the present work the magnetic and electronic properties of $GdRhIn_5$ were investigated. The compound crystallizes with the $HoCoGa_5$ type structure, space group $P4/mmm$. The antiferromagnetic ordering of this compound was confirmed, and the Néel temperature $\mathrm{T_N} = 41.0(2)$ was determined by AC magnetic susceptibility measurements. Magnetic and ^{155}Gd Mössbauer spectroscopic results point to a simple collinear aniferromagnetic structure with gadolinium moments aligned in- or close to the basal plane. The observed excess effective moment was mainly ascribed to the magnetic contribution of Gd 5*d*-electrons. The implication of the negative sign of the quadrupole interaction constant ΔE_{Q} on the sign of the axial B_2^0 crystal-field parameter and its consequences concerning the easy direction of the rare earth magnetic moments in the *RE*$\mathrm{RhIn_5}$ series were discussed in detail. A consistent description of the magnetic properties and the magnetic interactions was obtained in the framework of the simple two-sublattice molecular field approximation.

Acknowledgements

We thank the Degussa-Hüls AG for a generous gift of rhodium powder. This work was supported by the Deutsche Forschungsgemeinschaft through SPP 1166 *Lanthanoidspezifische Funktionalitäten in Molekül und Material*. V. I. Z. is indebted to the Alexander-von-Humboldt Foundation for a research stipend.

[1] Yu. N. Grin, Ya. P. Yarmolyuk, E. I. Gladyshevskii, Sov. Phys. Crystallogr. **24**, 137 (1979); Krystallografiya **24**, 242 (1979).
[2] Ya. M. Kalychak, V. I. Zaremba, V. M. Baranyak, V. A. Bruskov, P. Yu. Zavalij, Metally **1**, 209 (1989) (in Russian).
[3] H. Hegger, C. Petrovic, E. G. Moshopoulou, M. F. Hundley, J. L. Sarrao, Z. Fisk, J. D. Thompson, Phys. Rev. Lett. **84**, 4986 (2000).
[4] J. D. Thompson, R. Movshovich, Z. Fisk, F. Bouquet, N. J. Curro, R. A. Fisher, P. C. Hammel, H. Hegger, M. F. Hundley, M. Jaime, P. G. Pagliuso, C. Petrovic, N. E. Philips, J. L. Sarrao, J. Magn. Magn. Mater. **226 – 230**, 5 (2001).
[5] C. Petrovic, P. G. Pagliuso, M. F. Hundley, R. Movshovich, J. L. Sarrao, J. D. Thompson, Z. Fisk, P. Monthoux, J. Phys.: Condens. Matter **13**, L337 (2001).
[6] C. Petrovic, R. Movshovich, M. Jaime, P. G. Pagliuso, M. Ḟ. Hundley, J. L. Sarrao, Z. Fisk, J. D. Thompson, Europhys. Lett. **53**, 354 (2001).
[7] E. G. Moshopoulou, Z. Fisk, J. L. Sarrao, J. D. Thompson, J. Solid State Chem. **158**, 25 (2001).
[8] Ya. M. Kalychak, V. I. Zaremba, R. Pöttgen, M. Lukachuk, R.-D. Hoffmann, Rare Earth-Transition Metal-Indides, in K. A. Gschneidner (Jr.), J.-C. Bünzli, V. K. Pecharsky (eds): Handbook on the Chemistry and Physics of Rare Earths, in press.
[9] P. G. Pagliuso, J. D. Thompson, M. F. Hundley, J. L. Sarrao, Phys. Rev. B **62**, 12266 (2000).
[10] P. G. Pagliuso, J. D. Thompson, M. F. Hundley, J. L. Sarrao, Z. Fisk, Phys. Rev. B **63**, 054426 (2001).
[11] V. I. Zaremba, U. Ch. Rodewald, R.-D. Hoffmann, Ya. M. Kalychak, R. Pöttgen, Z. Anorg. Allg. Chem. **629**, 1157 (2003).
[12] V. I. Zaremba, U. Ch. Rodewald, R. Pöttgen, Z. Naturforsch. **58b**, 805 (2003).
[13] V. I. Zaremba, Ya. Galadzhun, D. Kaczorowski, M. Wolcyrz, 13th International Conference on Solid Compounds of Transition Elements, Stresa (Italy), April 2000, Abstract P-C56.
[14] D. Kußmann, R.-D. Hoffmann, R. Pöttgen, Z. Anorg. Allg. Chem. **624**, 1727 (1998).
[15] K. Yvon, W. Jeitschko, E. Parthé, J. Appl. Crystallogr. **10**, 73 (1977).
[16] G. Czjzek, Kernforschungszentrum Karlsruhe, unpublished.
[17] G. J. Long, T. E. Cranshaw, G. Longworth, Mössbauer Effect Reference and Data Journal **6**, 42 (1983).
[18] K. Tomala, G. Czjzek, J. Fink, H. Schmidt, Solid State Commun. **24**, 857 (1977).
[19] H. Armon, E. R. Bauminger, S. Ofer, Phys. Lett. **43B**, 380 (1973).

[20] K. Łątka, Magnetism and Hyperfine Interactions in GdT_2Si_2 Systems, Chapt. 5, p. 68, Report No1443/PS, Institute of Nuclear Physics, Cracow (1989).
[21] G. Czjzek, V. Oestreich, H. Schmidt, K. Łątka, K. Tomala, J. Magn. Magn. Mater. **79**, 42 (1989).
[22] R.-D. Hoffmann, R. Pöttgen, Th. Fickenscher, C. Felser, K. Łątka, R. Kmieć, Solid State Sci. **4**, 609 (2002).
[23] K. Łątka, Z. Tomkowicz, R. Kmieć, A. W. Pacyna, R. Mishra, Th. Fickenscher, R.-D. Hoffmann, R. Pöttgen, J. Solid State Chem. **168**, 331 (2002).
[24] D. H. Martin, Magnetism in Solids, p. 252 – 264, The M.I.T. Press, Massachusetts Institute of Technology, Cambridge, Massachusetts (1967).
[25] G. Czjzek, in G. J. Long, F. Grandjean (eds.): Mössbauer Spectroscopy Applied to Magnetism and Materials Science, Vol. 1, p. 373, Plenum Press, New York (1993).
[26] Y. Tanaka, D. B. Laubacher, R. M. Steffen, E. B. Shera, H. D. Wohlfahrt, M. V. Hoehn, Phys. Lett. **108B**, 8 (1982).
[27] E. R. Bauminger, G. M. Kalvius, F. E. Wagner, in G. K. Shenoy, F. E. Wagner (eds): Mössbauer Isomer Shifts, p. 661, North Holland Publishing Company, Amsterdam, New York, Oxford (1978).
[28] J. E. Greedan, V. U. S. Rao, J. Solid State Chem. **6**, 387 (1973).
[29] J. Jensen, A. R. Mackintosch, Rare Earth Magnetism, Clarendon Press, Oxford (1991).
[30] W. E. Wallace, S. G. Sankar, V. U. S. Rao, in J. D. Dunitz, P. Hemmerich, J. A. Ibers, C. K. Jørgensen, J. B. Neilands, D. Reinen, R. J. P. Williams (eds.): Structure and Bonding, Vol. 33, p. 1, Springer, Berlin (1997).
[31] R. E. Watson, A. J. Freeman, in A. J. Freeman, R. B. Frankel (eds): Hyperfine Interactions, p. 53, Academic Press, New York (1967).
[32] R. E. Gegenwarth, J. I. Budnick, S. Skalski, J. H. Wernick, Phys. Rev. Lett. **18**, 9 (1967).
[33] J. S. Smart, Effective Field Theories of Magnetism, p. 62, W. B. Saunders, Philadelphia and London (1966).
[34] S. Foner, in G. T. Rado, H. Suhl (eds): Magnetism, p. 385 – 390, Academic Press, New York and London (1963).
[35] S. E. Barnes, K. Baberschke, M. Hardiman, Phys. Rev. **18B**, 2409 (1978).
[36] Y. Shapira, J. Appl. Phys. **42**, 1588 (1971).